Applied Mathematical Modelling 39 (2015) 5783–5790

Contents lists available at ScienceDirect

Applied Mathematical Modelling

journal homepage: www.elsevier.com/locate/apm

Image hiding in time-averaged moiré gratings on finite element grids ☆

M. Vaidelys, J. Ragulskiene, S. Aleksiene, M. Ragulskis *

Research Group for Mathematical and Numerical Analysis of Dynamical Systems, Kaunas University of Technology, Studentu 50, Kaunas LT-51368, Lithuania

ARTICLE INFO

Article history:
Received 24 February 2014
Received in revised form 7 October 2014
Accepted 27 January 2015
Available online 7 February 2015

Keywords:
Dynamic visual cryptography
Time-averaged moiré
Cover image
Eigen-mode

ABSTRACT

Image hiding scheme based on time-averaged moiré fringes on finite element grids is proposed in this paper. This visual communication scheme is based on the formation of time-averaged moiré fringes in the digital dichotomous cover image when it is oscillated according to a predefined Eigen-shape. Initial phase scrambling and phase normalization algorithms are used to encode the secret in the cover image. Theoretical relationships between the amplitude of the Eigen-shape, the order of the time-averaged moiré fringe and the pitch of the deformable one-dimensional moire grating are derived. Computational experiments are used to illustrate the efficiency and applicability of this image hiding scheme in practical applications.

1. Introduction

Visual cryptography was introduced in 1994 by Noar and Shamir [1]. It encrypts visual information in such a way that the decryption is completely visual and computers are not required to interpret the secret image. Visual cryptography is a secret sharing scheme. The secret image is broken up into several shares which are printed on separate transparencies. The decryption is performed by overlaying the shares. Many advances have been done in visual cryptography since 1994. Color image visual cryptography is proposed in [2,3]; visual cryptography with the ideal contrast scheme is introduced in [4]. Multi-secret visual cryptography is presented in [5]; visual cryptography with incrementing functionality is introduced in [6]. Visual cryptography schemes enabling cheating prevention are proposed in [7].

The concept of dynamic visual cryptography was introduced in [8]. This method is based not on static superposition of shares, but on time-average geometric moiré applied for a single encoded image. The secret image is embedded into the stochastic moiré grating; the secret is leaked only when the amplitude of the harmonic oscillations is set to a preselected value. A naked eye cannot interpret the secret image from the stationary cover image. Therefore, dynamic visual cryptography is similar to classical visual cryptography – special algorithms are required to encode the image, but decoding is completely visual. Additional image security measures are implemented in [9,10], where the secret image is leaked in a form of a pattern of time-averaged moiré fringes only when the encrypted cover image is oscillated according to a predefined law of motion.

An alternative image hiding scheme based on deformable moiré gratings is proposed in [11]. The secret image is leaked from the cover image not when it is oscillated according to a pre-determined law of motion – but when it is deformed along

☆ 2013 International Applied Science and Precision Engineering Conference, October 2013 NanTou, Taiwan.

* Corresponding author. Tel.: +370 698 22456.
E-mail addresses: martynas.vaidelys@ktu.lt (M. Vaidelys), jurate.ragulskiene@ktu.lt (J. Ragulskiene), sandra.aleksiene@ktu.lt (S. Aleksiene), minvydas.ragulskis@ktu.lt (M. Ragulskis).

http://dx.doi.org/10.1016/j.apm.2015.01.056
0307-904X/

the longitudinal coordinate of the stochastic moiré grating. Such implementation requires a special strategy for the formation of the cover image and opens new possibilities for optical control of vibrating structures [11]. A natural extension of such image hiding technique would be a dynamic visual cryptography scheme based on harmonic oscillations of the deformable moiré grating according to a pre-selected Eigen-shape of an elastic structure. In other words, the stochastic cover image must be formed on the surface of an elastic structure – and the secret image would be leaked only if this structure is vibrated according to a pre-specified Eigen-shape. Such image hiding schemes would open new possibilities for optical control of MOEMS (micro-opto-electro-mechanical systems) where a stochastic cover moiré image could be formed on the surface of the cantilever or diaphragm. The secret image would be leaked when the micro-structure would oscillate at predetermined law of motion. The main objective of this manuscript is to build the mathematical foundation for the formation of cover images for such demanding applications. This paper is organized as follows.

Optical relationships are discussed in Section 2; the construction of a deformable moiré grating is presented in Section 3; the DVC scheme based on deformable gratings is illustrated in Section 4; concluding remarks are given in Section 5.

2. Preliminaries

Let us consider a one-dimensional harmonic moiré grating:

$$F(x) = \frac{1}{2} + \frac{1}{2}\cos\left(\frac{2\pi}{\lambda}x\right), \tag{1}$$

where x is the longitudinal coordinate; λ is the pitch of the grating; the numerical value 0 corresponds to the black color; 1 – to the white color and all intermediate values correspond to an appropriate grayscale level. Let the moiré grating be formed on the surface of a one-dimensional deformable body. Let the deformation from the state of equilibrium at the point x at time moment t is equal to $u(x,t)$. Then the deformed moiré grating can be expressed in the explicit form:

$$F(x,t) = \frac{1}{2} + \frac{1}{2}\cos\left(\frac{2\pi}{\lambda}\mu(x,t)\right), \tag{2}$$

if only the independent variable x can be explicitly expressed from the relationship:

$$x + u(x,t) = z, \tag{3}$$

into the form:

$$x = \mu(z,t). \tag{4}$$

Let us assume that the function $u(x,t)$ does describe a harmonic oscillation around the state of equilibrium:

$$u(x,t) = a(x)\sin(\omega t + \varphi), \tag{5}$$

where $a(x)$ is the Eigenshape of in-plane oscillations; ω and φ are the circular frequency and the phase of harmonic oscillations.

Let us linearize the function $a(x)$ around the point x_0:

$$a(x) = a_0 + \dot{a}_0(x - x_0) + O(x - x_0)^2, \tag{6}$$

where $a_0 = a(x_0)$; $\dot{a}_0 = \frac{da(x)}{dx}\Big|_{x=x_0}$. Without losing the generality we assume that $\omega = 1$ and $\phi = 0$. Then, Eq. (4) yields:

$$x = \frac{z - a_0\sin t + \dot{a}_0 x_0 \sin t}{1 + \dot{a}_0 \sin t}. \tag{7}$$

Thus, the grayscale level of the deformed moiré grating at coordinate x at time moment t reads:

$$F(x,t) = \frac{1}{2} + \frac{1}{2}\cos\left(\frac{2\pi}{\lambda}\cdot\frac{x + (\dot{a}_0 x_0 - a_0)\sin t}{1 + \dot{a}_0\sin t}\right). \tag{8}$$

2.1. Non-deformable moiré grating

Let us assume that $a(x) = A$ (A is a constant). In other words, the deflection $u(x,t) = A\sin(\omega t + \varphi)$ describes the oscillation of a non-deformable body around the state of equilibrium [8]. Then the instantaneous grayscale level of the moiré grating reads:

$$F(x,t) = \frac{1}{2} + \frac{1}{2}\cos\left(\frac{2\pi}{\lambda}\cdot(x - A\sin(\omega t + \varphi))\right). \tag{9}$$

Now, let us assume that time-averaging techniques are used to register the image of the oscillating moiré grating [8,12]:

$$\lim_{T\to\infty}\frac{1}{T}\int_0^T F(x,t)dt = \frac{1}{2} + \frac{1}{2}\cos\left(\frac{2\pi}{\lambda}x\right)J_0\left(\frac{2\pi}{\lambda}A\right), \tag{10}$$

where J_0 is the zero order Bessel function of the first kind. Note that the distribution of the grayscale level in the time-averaged image does not depend on the frequency and on the phase of harmonic oscillations.

Time-averaged moiré fringes form when $J_0 = 0$. That happens at amplitudes $\frac{2\pi}{\lambda}A_k = r_k$, where r_k are roots of J_0; $k = 1, 2, \ldots$. The formation of time-averaged fringes is illustrated in Fig. 1. The x-axis in Fig. 1 stands for the longitudinal coordinate x; the y-axis – for the amplitude A. A sharp high-contrast harmonic moiré grating is visible at $A = 0$; gray time-averaged fringes are clearly visible at the amplitudes corresponding to the roots r_k (Fig. 1). One-dimensional moiré grating is formed only in a finite interval in Fig. 1 – blurred zones around the ends of that interval do occupy a region proportional to the amplitude of harmonic oscillations.

2.2. Deformable moiré grating; linear deformation field

Let us assume that $a(x) = Ax$. The deflection from the state of equilibrium is now proportional to the coordinate x. In other words, harmonic moiré grating can be formed on the surface of one-dimensional body in the state of equilibrium – but the moiré grating will be deformed when the body will perform oscillations in time. That is the principal difference from non-deformable moiré gratings (described in Section 2.1) where the oscillation of the non-deformable one-dimensional body is considered around the state of equilibrium and the moiré grating is not deformed.

Linearization around x_0 yields: $a(x) = Ax_0 + A(x - x_0)$; $a_0 = Ax_0$; $\dot{a}_0 = A$. Thus, Eq. (8) reads:

$$F(x,t) = \frac{1}{2} + \frac{1}{2}\cos\left(\frac{2\pi}{\lambda}\frac{x}{1 + A\sin t}\right) = \frac{1}{2} + \frac{1}{2}\cos\left(\frac{2\pi x}{\lambda}\left(1 - A\sin t + O\left(A^2\right)\right)\right) \approx \frac{1}{2} + \frac{1}{2}\cos\left(\frac{2\pi}{\lambda}x - \frac{2\pi}{\lambda}Ax\sin t\right). \quad (11)$$

Note that $0 < A \ll 1$ (a singularity occurs at $A = 1$ in Eq. (11)). Finally, the time-averaged image reads [11]:

$$\begin{aligned}\lim_{T\to\infty}\frac{1}{T}\int_0^T F(x,t)dt &= \frac{1}{2} + \frac{1}{2}\cos\left(\frac{2\pi}{\lambda}x\right)\lim_{T\to\infty}\frac{1}{T}\int_0^T \cos\left(\frac{2\pi}{\lambda}Ax\sin t\right)dt = \frac{1}{2} + \frac{1}{2}\cos\left(\frac{2\pi}{\lambda}x\right)\lim_{T\to\infty}\frac{1}{T}\int_0^T e^{i\frac{2\pi}{\lambda}Ax\sin t}dt \\ &= \frac{1}{2} + \frac{1}{2}\cos\left(\frac{2\pi}{\lambda}x\right)J_0\left(\frac{2\pi}{\lambda}Ax\right). \quad (12)\end{aligned}$$

Thus, time-averaged moiré fringes form at $\frac{2\pi}{\lambda}Ax = r_k$; $k = 1, 2, \ldots$ (Fig. 2). The oscillating moiré grating is shown in the left upper image. The left side of the one-dimensional moiré grating is motionlessly fixed; the right side of the deformed grating does oscillate at a preset amplitude $A^* = 0.05$, the pitch of the moire grating at the state of equilibrium is $\lambda = 0.015$. The left bottom part of Fig. 2 does represent the time-averaged image of the one-dimensional grating at $A^* = 0.05$; time-averaged moiré fringes can be clearly seen in this image. The right part of Fig. 2 shows the time-averaged images of the one-dimensional moiré grating at increasing amplitudes A (the higher is the amplitude of harmonic oscillations, the larger number of moiré fringes is visible in the time-averaged image). The horizontal dashed line represents the amplitude $A^* = 0.05$.

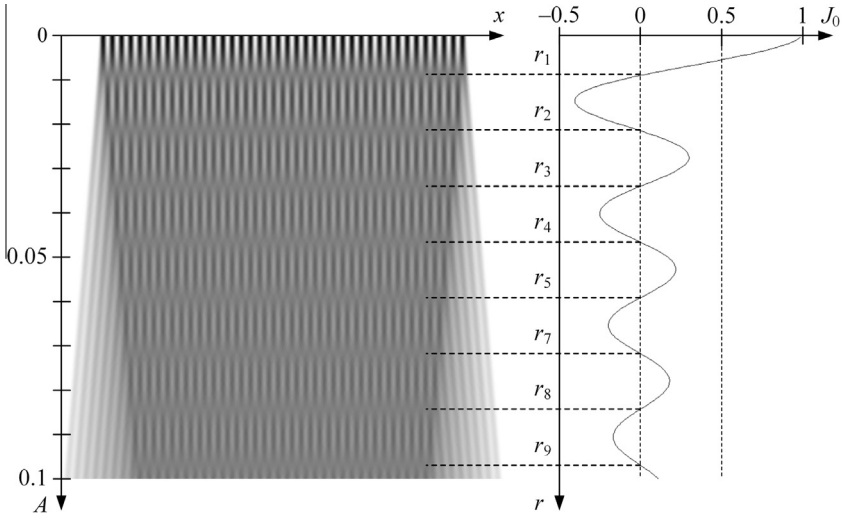

Fig. 1. Harmonic oscillation of the inelastic one-dimensional moiré grating ($\lambda = 0.025$) produces time-averaged fringes. Time-averaged image is shown on the left; the graph of J_0 – at the right part of the figure.

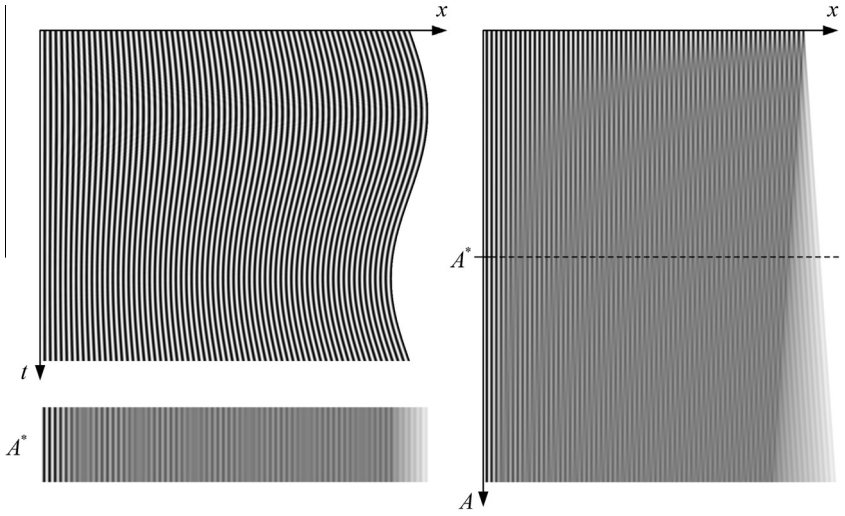

Fig. 2. Harmonic oscillation of the deformable one-dimensional moiré grating ($\lambda = 0.015$) also produces time-averaged fringes. One period of harmonic oscillations is illustrated in the top left image; one-dimensional time-averaged image at $A^* = 0.05$ is shown at the bottom on the left; the formation of time-averaged fringes at increasing amplitudes is illustrated on the right; $A = [0.001, 0.1]$.

3. Deformable moiré grating; nonlinear deformation field

The main objective of this paper is to develop an image hiding scheme based on deformable moiré gratings on finite element grids. In other words, deformation field $a(x)$ must be a nonlinear function. That requires the development of a complex inverse problem.

Let us construct this inverse problem for the general case described by Eq. (8). In other words – what should be the distribution of the pitch of the one-dimensional moiré grating $\lambda(x)$ that the whole time-averaged image would be transformed into a time-averaged fringe – regardless of the function $a(x)$.

Without losing the generality we assume that $x_0 = 0$. Let us denote $\bar{a}(x) = a_0 + \dot{a}_0 x$. Then, Eq. (8) reads:

$$\begin{aligned} F(x,t) &= \frac{1}{2} + \frac{1}{2}\cos\left(\frac{2\pi}{\lambda}\cdot\frac{x - a_0\sin t}{1 + \dot{a}_0\sin t}\right) \approx \frac{1}{2} + \frac{1}{2}\cos\left(\frac{2\pi}{\lambda}(x - a_0\sin t)(1 - \dot{a}_0\sin t)\right) \\ &= \frac{1}{2} + \frac{1}{2}\cos\left(\frac{2\pi}{\lambda}\left(\left(x + a_0\dot{a}_0\sin^2 t\right) - (a_0 + \dot{a}_0 x)\sin t\right)\right) \\ &= \frac{1}{2} + \frac{1}{2}\cos\left(\frac{2\pi}{\lambda}\left(x + a_0\dot{a}_0\sin^2 t\right)\right)\cos\left(\frac{2\pi}{\lambda}\bar{a}(x)\sin t\right) + \frac{1}{2}\sin\left(\frac{2\pi}{\lambda}\left(x + a_0\dot{a}_0\sin^2 t\right)\right)\sin\left(\frac{2\pi}{\lambda}\bar{a}(x)\sin t\right). \end{aligned} \tag{13}$$

Note that $\lim_{T\to\infty}\frac{1}{T}\int_0^T \sin\left(\frac{2\pi}{\lambda}(x\dot{a}_0 + a_0)\sin t\right)dt = 0$ due to the oddness of the sine function. Also, $\lim_{T\to\infty}\frac{1}{T}\int_0^T \sin^2 t\,dt = 0.5$. Then, the time-averaged image reads:

$$\begin{aligned} \lim_{T\to\infty}\frac{1}{T}\int_0^T F(x,t)dt &\approx \frac{1}{2} + \frac{1}{2}\cos\left(\frac{2\pi}{\lambda}\left(x + \frac{1}{2}a_0\dot{a}_0\right)\right)\lim_{T\to\infty}\frac{1}{T}\int_0^T \cos\left(\frac{2\pi}{\lambda}\bar{a}(x)\sin t\right)dt \\ &= \frac{1}{2} + \frac{1}{2}\cos\left(\frac{2\pi}{\lambda}\left(x + \frac{1}{2}a_0\dot{a}_0\right)\right)\lim_{T\to\infty}\frac{1}{T}\int_0^T e^{i\frac{2\pi}{\lambda}\bar{a}(x)\sin t}dt \\ &= \frac{1}{2} + \frac{1}{2}\cos\left(\frac{2\pi}{\lambda}\left(x + \frac{1}{2}a_0\dot{a}_0\right)\right)J_0\left(\frac{2\pi}{\lambda}\bar{a}(x)\right). \end{aligned} \tag{14}$$

Thus, time averaged moiré fringes form at $\frac{2\pi}{\lambda}\bar{a}(x) = r_k;\ k = 1, 2, \ldots$. This equality corresponds well to the results produced in Sections 2.1 and 2.2 – but is far from being trivial and does not follow directly from the formulation of the problem. Note that the linearization is now performed at a preselected coordinate x – while the whole field of amplitudes was linear by the definition in Section 2.2. A successful implementation of a DVC scheme requires that a preselected area of the cover image would be transformed into a uniform time-averaged moir fringe. The only controlled parameter of the cover image is the pitch $\lambda(x)$. Eq. (14) suggests that the distribution of the pitch should read:

$$\lambda(x) = \frac{2\pi}{r_k}\bar{a}(x); \quad k = 1, 2, \ldots \tag{15}$$

Relationship (15) does comprise the linearized field of amplitudes $\bar{a}(x)$. We will use computational tools to test the conjecture that $\bar{a}(x)$ can be replaced by $a(x)$ in Eq. (15).

Let us assume that a one-dimensional elastic structure oscillates according to the law:

$$u(x,t) = 0.1\sin(\pi x)\sin(\omega t + \varphi), \quad 0 \ll x \ll 1. \tag{16}$$

The above stated conjecture implies that a time-averaged moiré fringe must form in the whole domain of x when the stationary moiré grating with the pitch:

$$\lambda(x) = 0.1\frac{2\pi}{r_1}\sin(\pi x), \tag{17}$$

is oscillated according to the law described by Eq. (16). The parameter k is fixed to 1 because the contrast around the first time-averaged moiré fringe (the first root of J_0) is the highest.

Note that the construction of a stationary moiré grating according to relationship (17) is a not very complex computational exercise – except the regions around the boundaries where the pitch of the grating quickly converges to zero and the size of the pixel is not small enough to represent the grayscale oscillation of the grating (as illustrated at the left side of Fig. 3). Now, instead of applying the oscillations of the moiré grating according to Eq. (16) we set the oscillation law to:

$$u(x,t) = b\sin(\pi x)\sin(\omega t + \varphi), \quad 0 \ll x \ll 1, \tag{18}$$

where the parameter b is varied from 0 to 0.2 (Fig. 3). It can be clearly seen that the time-averaged moiré fringe forms at $b = 0.1$. Thus, the conjecture stating that the linearized field $\bar{a}(x)$ can be replaced by $a(x)$ in Eq. (15) does hold even for such a complex non-linearized law of motion described by Eq. (16).

4. Dynamic visual cryptography based on deformable moiré gratings on finite element grids

As mentioned previously, nonlinear deformation fields will be used for the formation of time-averaged moiré fringes. Since one-dimensional moiré gratings have been used so far, the 2D field of deformations $a(x,y)$ determined by FEM computations are sliced horizontally, and one-dimensional pitch distributions are computed in adjacent moir gratings. Therefore, every row of pixels in the digital image of 2D deformations is interpreted as a separate one-dimensional variation of amplitudes $a(x)$. This process is illustrated in Fig. 4.

Fig. 4a shows the twelfth Eigen-shape of a plate – dark zones stand for maximum deformations from the state of equilibrium – white zones stand for regions which do not oscillate at this resonance frequency. First of all, the maximum amplitude of oscillation must be set at the point of maximal deformations – the Eigen-shape is multiplied by a pre-determined constant. The next step is the formation of an array of one-dimensional moiré gratings. The resolution of Fig. 4a is 500×500 pixels. Thus, 500 horizontal one-dimensional moiré gratings are formed in Fig. 4b and the variation of the pitch in the domain of the grating is constructed according to Eq. (15). The only exception is that the linearized deformation field $\bar{a}(x)$ is replaced by $ka(x) + b$ where $a(x)$ is the numerical values of the Eigen-shapes in the current grating and k, b are positive constants greater than 0. The constant b is required in order to avoid singularities at the points where the amplitudes $a(x)$ become equal to 0; k is required for the control of the range of numerical values of amplitudes. We set $k = 0.0025$ and

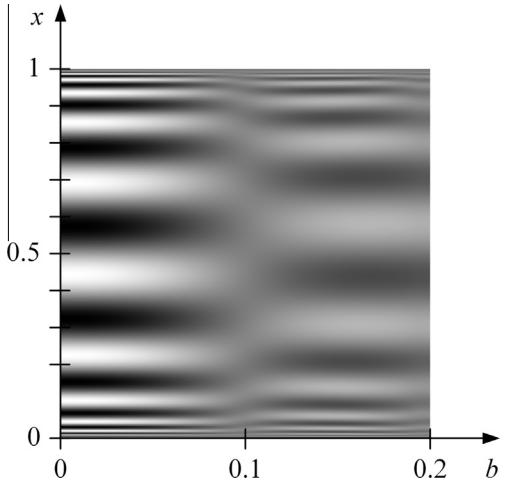

Fig. 3. Time-averaged image of the one-dimensional grating (the variation of the pitch is determined according to Eq. (17)); the variation of the amplitude b is determined by Eq. (18).

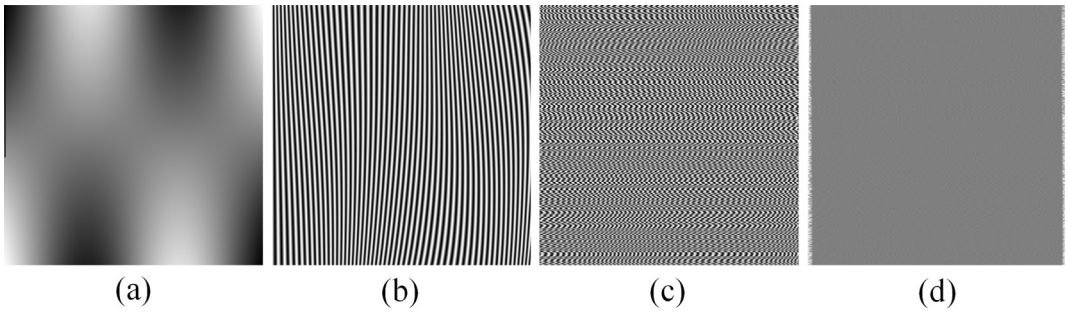

Fig. 4. Harmonic oscillations according to the 12th Eigen-mode of a free rectangular plate produce a gray two-dimensional image; part (a) shows the Eigen-shape; part (b) illustrates the stationary moiré grating (the pitch of the grating varies in the interval $\lambda = [0.013, 0.026]$; $\lambda(x) = \frac{2\pi}{r_1} a(x)$); part (c) shows the cover image produced from the moiré grating; part (d) illustrates the time-averaged image when the cover image is oscillated according the 12th Eigen-mode.

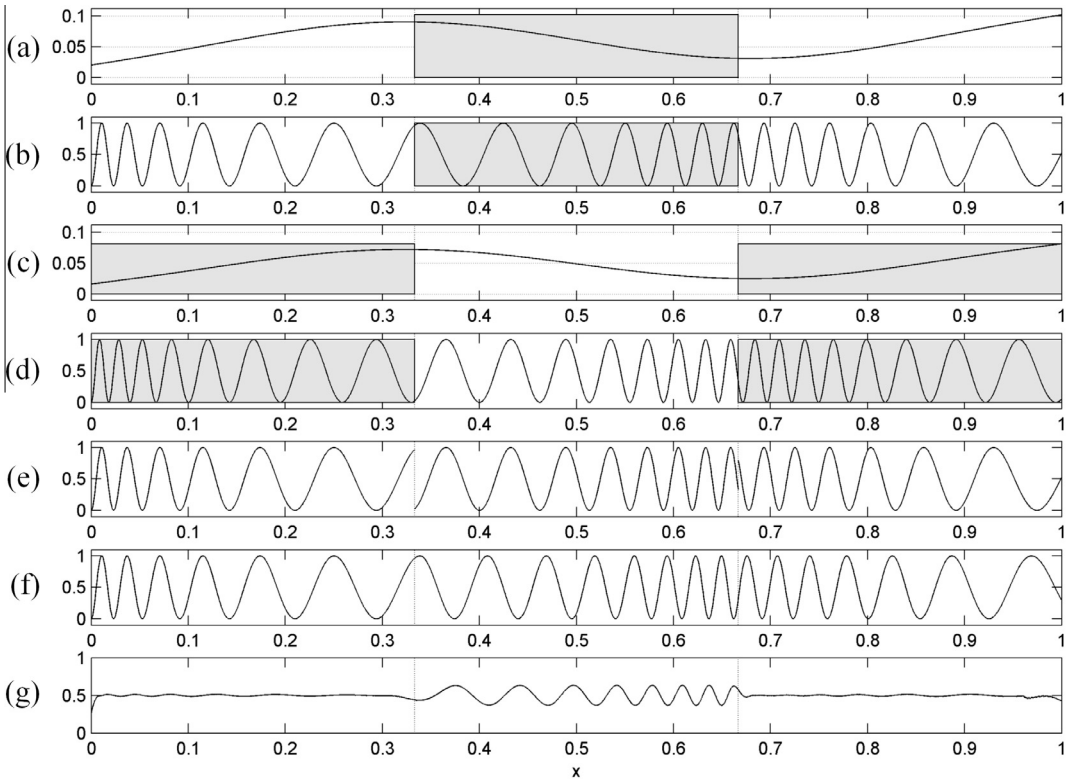

Fig. 5. A schematic diagram illustrating the encoding of the secret in a one-dimensional moiré grating. Part (a) shows the field of amplitudes $a(x)$ (according to a predefined Eigen-mode); part (b) illustrates the corresponding moiré grating. Part (c) shows the field of amplitudes used in the regions occupied by the secret; part (d) illustrates the corresponding moiré grating. The composite moire grating uses the left and the right thirds from part (b) and the middle third from part (d). All discontinuities in part (e) are eliminated by the phase regularization algorithm (part (f)). The time-averaged image of (f) is shown in part (g).

$b = 0.0075$ in all further computations – thus the initial range of the Eigen-mode $[-1, 1]$ is transformed into the working range of amplitudes $[0.005, 0.01]$.

Note that the initial phase of all 500 one-dimensional gratings is set to 0 – thus the image in Fig. 4b represents an interpretable array of lines which can reveal the Eigen-shape itself. The stochastic initial phase deflection algorithm [8] is used to confuse the image – the resulting image is shown in Fig. 4c. Note that the variation of the pitch in every single one-dimensional grating is not altered in the process.

Now, in-plane unidirectional oscillations according to the x-axis produce time-averaged moire fringes in the domain of every one-dimensional grating – the resulting image in Fig. 4d is completely gray (except the right and left boundaries where the image becomes slightly uneven).

The secret image is embedded into the cover image by modifying the phase regularization algorithm introduced in [8]. The functionality of this algorithm is illustrated in Fig. 5. Let us assume that the variation of the amplitude $a(x)$ is described in Fig. 5a. The corresponding grayscale level of the one-dimensional moire grating is illustrated in Fig. 5b. Let us assume that the "secret" information must be placed in the middle part of the grating. In other words, time-averaged moire fringe should form everywhere, except at the region occupied by the middle interval. The field of amplitude governing the harmonic oscillation of the moire grating is altered by multiplying it by a constant C little lower (or higher) that 1. The variation of the amplitude $a(x)$ in Fig. 5c is exactly the same as in Fig. 5a – except it is multiplied by $C = 0.8$; the corresponding moire grating is shown in Fig. 5d.

Now, the left third and the right third of the grating in Fig. 5b is copied to the composite grating illustrated in Fig. 5e. Such direct copying results into a non-continuous grating. The phase jumps at the joining points are eliminated by an appropriate selection of the phase of the grayscale level. Note that the variation of the pitch is not altered in the process (Fig. 5f). Finally, time-averaging of Fig. 5f results into Fig. 5g as it is oscillated by the law defined by Eq. (4) and the field of amplitudes $a(x)$ is

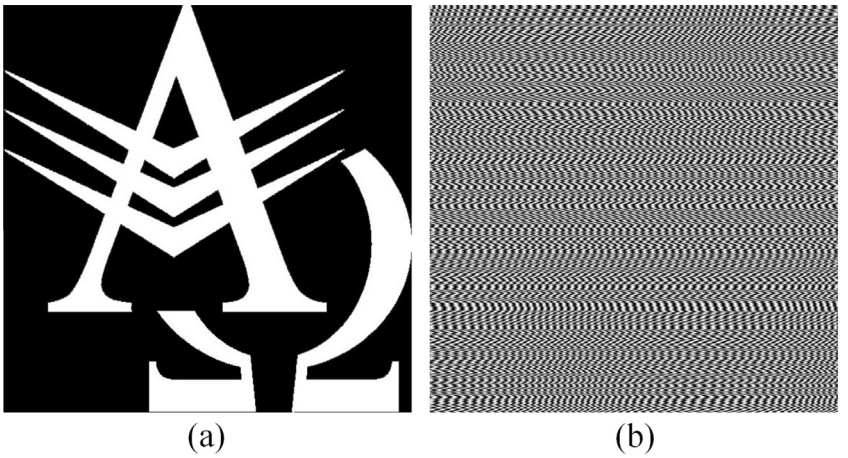

Fig. 6. The secret image is shown in part (a); the static cover image with the embedded secret (in such a way that the secret image would leak when the cover image is oscillated according to the 12th Eigen-mode) is shown in part (b) (the range of the pitch is from 0.013 up to 0.026).

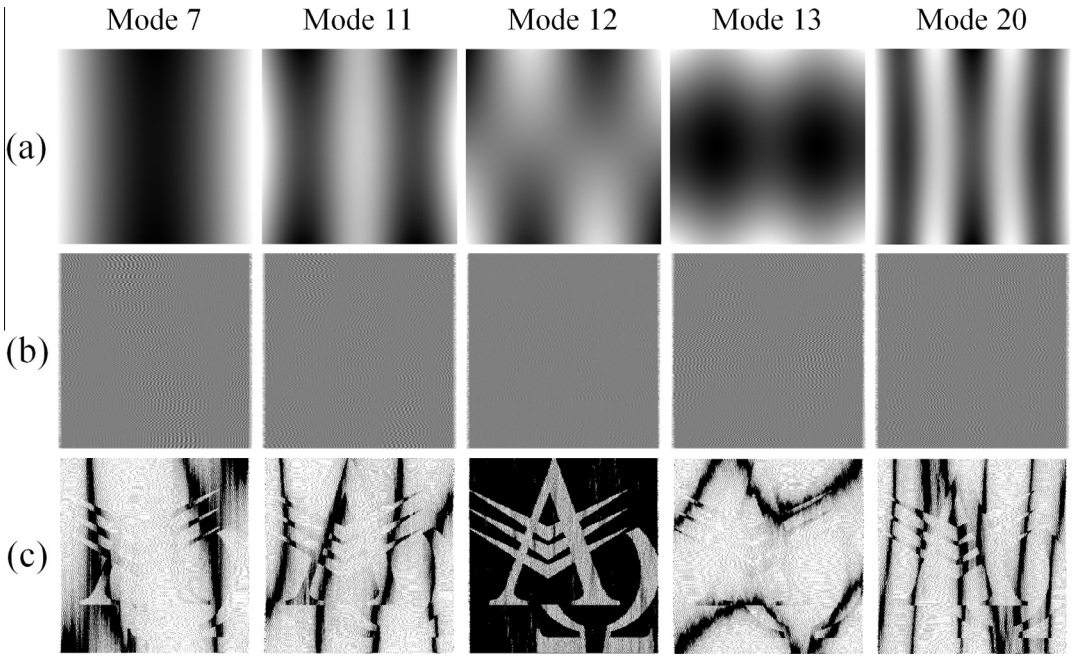

Fig. 7. The Eigen-mode serves as the key for visual decryption of the cover image. The first column shows different Eigen-shapes; the second column – time-averaged images; the third column – contrast enhanced time-averaged images.

determined by Fig. 5a. Time-averaged moire fringes form in the left-third and the right-third of the image; the middle-third of the time-averaged image does clearly stand out from the gray background.

Such image hiding scheme can be effectively used for embedding dichotomous images into the cover image. It is important to note that the Eigen-shape of the structure does serve as the secret key for visual decoding of the secret. In other words, the secret image does leak from the cover image only if it is oscillated according the Eigen-mode which was used to encode the image.

The following computation experiment is used to demonstrate the functionality of such image hiding scheme based on dynamic visual cryptography. The secret dichotomous image (shown in Fig. 6a) is embedded into the cover image (Fig. 6b) according to the twelfth Eigen-shape of the rectangular plate – stochastic initial phase and phase regularization algorithms are used to hide the secret. A naked eye could not identify the secret image from the cover image – moreover, the secret can be leaked only when the deformable cover image is oscillated according the Eigen-mode which was used to encode the secret.

In other words, the Eigen-mode itself can be considered as a key for the visual decoding procedure. Fig. 7 shows results of visual decoding when the cover image is oscillated according to different Eigen-modes; contrast enhancement procedures [13] are used to highlight moiré fringes in time-averaged images.

5. Conclusions

Image hiding scheme in time-averaged moiré gratings on finite element grids is presented in this paper. An image encoding scheme in deformable one-dimensional moiré gratings oscillating according to a predefined Eigen-mode is developed and implemented for the construction of two-dimensional digital dichotomous secret images. The secret is leaked from the cover image when it is oscillated according to a predefined Eigen-mode in a form of a pattern of time-averaged moiré fringes. The efficiency of the proposed scheme is illustrated by computational examples employing finite element grids.

Defects of the grid, defects of the material (or the geometry) of the FEM model could be considered as the next step in the security of this DVC scheme. Imagine a FEM grid (or the FEM model in general) with a micro-crack. It is well known that Eigen-modes can be exploited for the detection of micro-cracks. Thus, cover images could be constructed in such a way that the secret image would leak only if the FEM Eigen-mode would correspond to a structure with an exactly predefined micro-crack. The implementation of such a DVC scheme is a definite objective of the future research.

Acknowledgments

Financial support from the Lithuanian Science Council under project No. MIP-100/12 is acknowledged.

References

[1] M. Naor, A. Shamir, Visual cryptography, in: Advances in Cryptology–EUROCRYPT'94, Springer, 1995, pp. 1–12.
[2] Y.-C. Hou, Visual cryptography for color images, Pattern Recogn. 36 (7) (2003) 1619–1629.
[3] S. Cimato, R. Prisco, A. Santis, Colored visual cryptography without color darkening, in: C. Blundo, S. Cimato (Eds.), Security in Communication Networks, Lecture Notes in Computer Science, vol. 3352, Springer, Berlin Heidelberg, 2005, pp. 235–248.
[4] S. Cimato, A.D. Santis, A.L. Ferrara, B. Masucci, Ideal contrast visual cryptography schemes with reversing, Inf. Process. Lett. 93 (4) (2005) 199–206.
[5] C.-N. Yang, T.-H. Chung, A general multi-secret visual cryptography scheme, Opt. Commun. 283 (24) (2010) 4949–4962.
[6] R.-Z. Wang, Y.-C. Lan, Y.-K. Lee, S.-Y. Huang, S.-J. Shyu, T.-L. Chia, Incrementing visual cryptography using random grids, Opt. Commun. 283 (21) (2010) 4242–4249.
[7] Y.-C. Chen, D.-S. Tsai, G. Horng, A new authentication based cheating prevention scheme in naorshamirs visual cryptography, J. Visual Commun. Image Represent. 23 (8) (2012) 1225–1233.
[8] M. Ragulskis, A. Aleksa, Image hiding based on time-averaging moir, Opt. Commun. 282 (14) (2009) 2752–2759.
[9] M. Ragulskis, A. Aleksa, Z. Navickas, Image hiding based on time-averaged fringes produced by non-harmonic oscillations, J. Opt. A: Pure Appl. Opt. 11 (12) (2009) 125411.
[10] V. Petrauskiene, R. Palivonaite, A. Aleksa, M. Ragulskis, Dynamic visual cryptography based on chaotic oscillations, Commun. Nonlinear Sci. Numer. Simul. 19 (1) (2014) 112–120.
[11] R. Palivonaite, A. Aleksa, A. Paunksnis, A. Gelzinis, M. Ragulskis, Image hiding in time-averaged deformable moiré gratings, J. Opt. 16 (2) (2014) 025401.
[12] A. Kobayashi, Handbook on Experimental Mechanics, second ed., SEM, Bethel, 1993.
[13] M. Ragulskis, A. Aleksa, R. Maskeliunas, Contrast enhancement of time-averaged fringes based on moving average mapping functions, Opt. Lasers Eng. 47 (7–8) (2009) 768–773.